Journal of Photochemistry and Photobiology A: Chemistry 211 (2010) 170–175

Contents lists available at ScienceDirect

Journal of Photochemistry and Photobiology A: Chemistry

journal homepage: www.elsevier.com/locate/jphotochem

Location and catalytic role of iron species in TiO_2:Fe photocatalysts: An EPR study

Cristian Fàbrega[a,*], Teresa Andreu[a,b], Andreu Cabot[a,b], Joan Ramon Morante[a,b]

[a] EME/XaRMAE/IN UB, Dept. d'Electrònica, Universitat de Barcelona, C/Martí i Franquès 1, Planta 2, E-08028, Barcelona, Spain
[b] IREC, Catalonia Institute for Energy Research, E-08019, Barcelona, Spain

ARTICLE INFO

Article history:
Received 7 January 2010
Received in revised form 2 March 2010
Accepted 9 March 2010
Available online 15 March 2010

Keywords:
TiO_2
Iron doped
EPR
ESR
Methylene blue

ABSTRACT

A usual approach to improve the photocatalytic activity of wide band gap oxide semiconductors is through doping with transition metals. Dopants are primarily selected according to their capacity to introduce energy levels in the oxide band gap, promoting light absorbance. In the present work, we carefully characterize iron-doped titania powders obtained by a sol–gel route. Iron cations are introduced in the initial solution, before gelification, what promotes their lattice localization. X-ray diffraction and electron spin resonance spectroscopy are used to determine the temperature evolution of the crystalline structure and the dopant local environment. These results allow us to correlate the structural, electronic and chemical properties of the iron-doped titania powders with their activity towards the photocatalytic degradation of methylene blue (MB). The obtained results showed that Fe^{3+} cations far from improve the photocatalytic properties of bare TiO_2, decreased the activity towards methylene blue degradation. We associated such decrease with the role played by the iron cations depending on their position inside the lattice of TiO_2. And second, iron cations located near or at the surface tend to form iron-based structures, such as iron titanate or pseudobrookite which are highly inactive as photocatalyst.

1. Introduction

In recent years, titanium dioxide has been extensively investigated as an environmental harmonious and clean photocatalyst. Titania main advantages are its reasonable optical and electronic properties, a fair photocatalytic activity, and especially, its low cost, excellent chemical stability and non-toxicity [1,2]. However, its practical application has been limited by its low efficiency and wide band gap, which requires ultraviolet (UV) radiation as excitation source.

One usual approach to overcome these limitations is the modification of titania with transition metal additives [3,4]. Transition metals introduce electron energy states inside the titania band gap, which enhance its absorbance in the visible part of the spectrum. However, photocatalytic properties not only depend on the light absorbance, but they are also very sensitive to the dopant concentration, localization and chemical state of the dopant ions. As an example, while it is agreed that Fe^{3+} cations promote titania light absorbance by introducing shallow traps, its catalytic role during photooxidation processes still remains controversial [5–9]. Such a controversy arises from the different synthetic routes followed and the various post-synthesis processes used. This diversification on the processing methods has resulted in a large variety of iron chemical states and localization sites that make unfeasible a reliable comparison between previous works.

There are several strategies to introduce dopants into oxide-based catalyst. One can generally classify them into two main groups depending on the localization of the additive: (i) those that incorporate the additive at the oxide surface, such as impregnation [10–12] and (ii) those that incorporate the dopant ions inside the oxide lattice, such as sol–gel methods involving solid-solutions of the oxide and the doping ions [13–16].

The former approach seeks for the direct dopant introduction at the oxide surface [17,18]. In this strategy, the additional charges are photogenerated already at the oxide surface where the catalytic reaction takes place. However, its efficiency to introduce electron states inside the base-oxide band gap is limited. Impregnation usually results in a low yield of doping ions at substitutional lattice sites, while dopants mainly accumulate at the oxide surface forming independent clusters. As an example, the annealing of iron-impregnated TiO_2 leads to the formation of Fe_2TiO_3 or α-Fe_2O_3 at the TiO_2 surface [19]. The presence of these clusters is disadvantageous, since their photocatalytic activity is poor and they reduce the density of base-oxide surface sites for absorption and photocatalysis.

An alternative approach seeks a high yield of doping ions at substitutional lattice sites to maximize the outcoming density of shallow traps and thus of light absorbance. Because this approach does not particularly look for a surface localization of the dopant, its main drawback is the reduced yield of photogenerated carrier

* Corresponding author. Tel.: +34 934034804; fax: +34 934021148.
E-mail address: cfabrega@el.ub.es (C. Fàbrega).

1010-6030/$ – see front matter © 2010 Elsevier B.V. All rights reserved.
doi:10.1016/j.jphotochem.2010.03.003

reaching the oxide surface and participating on the catalytic reaction [8]. In this synthetic approach, a posterior thermal processing of the material aims for a dopant diffusion towards the oxide surface. Such thermal annealing process may result in a segregation of the dopants in independent clusters [19].

This second procedure has important technological advantages, such as the higher yield of isolated additive ions introduced and the significantly lower processing cost associated to the reduced number of processing steps involved. However, the complexity of the material characterization and the additional dependence of the final product on the processing steps, have resulted in a further degree of discrepancy among previously obtained results.

The present work aims to clarify the dependence on the annealing process of the chemical state and localization of iron cations in titania powders obtained by sol–gel. Using Electron Paramagnetic Resonance (EPR), we investigate the local environment of the iron cations incorporated in the titania lattice. Our data allows correlating the structural, electronic and surface properties of the semiconductor with its activity towards the photocatalytic degradation of methylene blue (MB).

2. Experimental

2.1. Materials

Fe-doped TiO_2 was synthesized using a sol–gel route. 25 ml of titanium isopropoxide (Alfa Aesar, 97%) were diluted in 145 ml of isopropanol. To this solution, different amounts (0.16, 0.33, 0.49 and 0.65% at.) of $Fe(NO_3)_3{\cdot}9H_2O$ (Aldrich, 99.99%) were added. The resulting mixture was hydrolyzed with 153 ml of acidic water (pH 3), stirred for 24 h, filtered and washed several times with deionised water. The final product was dried at 50 °C during 24 h. The resulting powder was annealed in air at different temperatures (200, 400, 500,550, 600 and 800 °C).

2.2. Characterization

XRD analysis was performed on a Bragg–Brentano PANalytical X'pert PRO diffractometer with monochromatized CuKα radiation (λ = 1.5406 Å) operating at 45 kV and 40 mA. Inductively coupled plasma optical emission spectrometry (ICP-OES) was carried out to quantify the iron content. The Brunauer–Emmett–Teller (BET) specific surface areas of the samples were determined through nitrogen adsorption at 77 K (Micromeritics Tristar 3000). The X-band EPR spectra were recorded at 77 K using a Bruker ESP300E spectrometer. The EPR spectrometer settings were: center field, 3105.100 G; sweep width, 6000 G; modulation amplitude, 31.985 G; sweep time, 83.886 s; microwave frequency, 9.79 GHz; microwave power, 1 mW; spectrometer gain, 1.00×10^4. UV–vis diffuse reflectance spectra (DRS) was recorded by a Shimadzu UV-2101 spectrometer equipped with an integrating sphere assembly, using $BaSO_4$ as reflectance sample.

The powders photocatalytic activity was evaluated by measuring decomposition rates of methylene blue under visible light irradiation (Solar Light Xe lamp 16S 300W with AM.0 and AM1.5 filters) at 150 mW/cm^2. A glass reactor consisting of a central walled glass surrounded by an outer glass jacket with water circulation (all the experiments were carried out at 25 °C) was filled with 200 ml of methylene blue solution (10 ppm) together with 0.25 g/l of catalyst powder suspension. The mixture was stirred in dark for 1 h in order to establish adsorption/desorption equilibrium of the methylene blue molecules onto de TiO_2 surface [20]. Afterwards, 10 ml of the suspension were sampled, the catalyst was removed by centrifugation and the solution absorbance, measured at 664 nm, was recorded in a PerkinElmer Lambda 35 UV–vis spectrometer. Then, the solar simulator was switched on, and the aqueous suspensions were irradiated from the top of the glass reactor. At given time intervals, 10 ml of the suspension were subsequently recovered, centrifuged and its light absorption was measured.

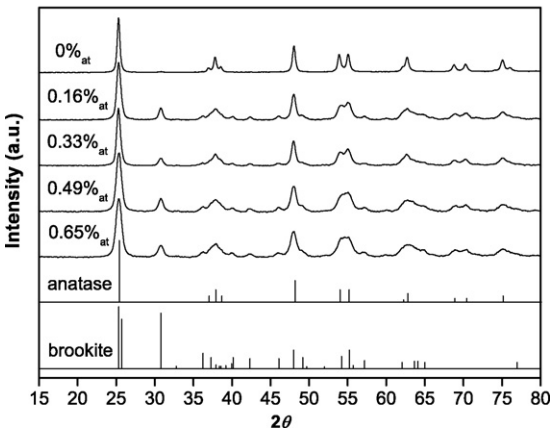

Fig. 1. X-ray powder diffraction spectra of iron-loaded samples calcined at 550 °C: 0%$_{at}$, 0.16%$_{at}$, 0.33%$_{at}$, 0.49%$_{at}$, 0.65%$_{at}$ of iron content and the corresponding diffraction pattern of anatase (21-1272) and brookite (29-1360) phases.

3. Results and discussion

3.1. XRD, ICP and BET

Figs. 1 and 2 show the evolution of the titania XRD spectra as a function of the iron loading (T = 550 °C) and annealing temperature (0.49%$_{at}$ sample), respectively. The phase concentrations and average crystallographic domain size estimated from the analysis of these diffractograms, along with the iron concentrations measured by ICP and specific surface area measurements (BET), were collected in Table 1. All samples showed a mixture of anatase (JCPDS 21-1272) and brookite (JCPDS 29-1360) phases. While there was no apparent dependence of the amount of brookite phase with the iron loading, only the undoped TiO_2 sample was composed of pure anatase phase. The presence of brookite diminished with the annealing temperature and, at 600 °C, the brookite concentration was residual (8%) and the rutile phase started to appear. At 800 °C, rutile (JCPDS 21–1276) was the dominant phase. However, a detailed analysis of the 800 °C annealed sample spectrum

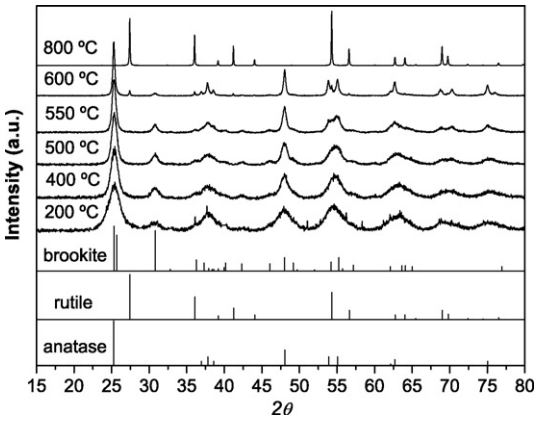

Fig. 2. X-ray powder diffraction spectra of TiO_2-Fe (0.49) sample at different heating temperatures (200, 400, 500, 550, 600, 800 °C) and the corresponding diffraction patterns of antase (21-1272), brookite (29-1360) and rutile 21-1276 phases.

Table 1
Phase composition[a], crystalline size[b] and BET measurements of TiO_2-Fe samples as function of iron content (550 °C) and annealing temperature (0.49%$_{at.}$).

	Phase Composition	BET (m^2/g)	Crystalline size (diameter in nm)		
			Anatase	Brookite	Rutile
TiO_2	A	19.58	22.8	–	–
TiO_2-0.16 (0.18)[c]	A, B (34%)	31.12	10.4	11.6	–
TiO_2-0.33 (0.35)[c]	A, B (31%)	30.45	11.3	12.7	–
TiO_2-0.49 (0.49)[c]	A, B (30%)	28.86	14.7	13.5	–
TiO_2-0.65 (0.60)[c]	A, B (34%)	26.35	14.3	15.9	–
TiO_2-400	A, B (35%)	79.20	7.9	8.1	–
TiO_2-500	A, B (39%)	45.91	10.5	9.8	–
TiO_2-550	A, B (30%)	28.86	14.7	13.5	–
TiO_2-600	A, B (8%)	2.61	29.3	15.4	50.3
TiO_2 800	R	2.17	–	–	85.2

[a] Phase composition is defined as the ration between the two main peaks area of anatase (A) and brookite (B) phase.
[b] Particle size was calculated with Scherrer equation by using the (1 0 1), (1 1 0) and (2 1 1) peaks appearing of anatase, rutile and brookite respectively.
[c] Experimental atomic percentage values obtained by ICP.

revealed a small trace of pseudobrookite phase (JCPDS 41-1432). We speculate that the presence of brookite seeded the formation of pseudobrookite in preference to haematite, by providing a crystallographic similar surface.

The average crystallographic domain sizes were calculated using the Scherrer equation from the fitting of the (1 0 1), (1 1 0) and (2 1 1) peaks corresponding to the anatase, rutile and brookite phases, respectively. We observed a clear influence of the presence of iron on the titania crystal size. The crystal size of pure TiO_2 was twice as large as those of the iron-loaded samples. Such an inhibition of the crystallographic domain growth and phase transformation due to the presence of transition metals inside the TiO_2 lattice is well documented in previous works [21].

The specific surface area of the samples with different iron loading was in the range of 26–31 m^2/g. This indicates that low levels of iron loading do not significantly influences the overall surface area. Note that BET measurements were directly related, as expected, to crystal domain size. Also, the addition of iron inhibits crystalline growth compared to the undoped sample. In contrast, the specific surface area was highly dependant on the annealing temperature, because of the rapid growth of the crystal domain. When the rutile phase started to appear at 600 °C, the specific surface area fell to 2 m^2/g, approximately.

Finally, note that the close similitude between the nominal dopant concentrations and the experimental values obtained from the ICP measurements, confirm the excellent efficiency of our synthetic route in incorporating iron into the TiO_2 lattice.

3.2. UV–vis DRS

The doped samples exhibit a color gradation ranging from yellow-orange at low dopant concentration to dark red at the highest iron loading. The color deepens as samples are processed at progressively higher temperatures.

Fig. 3 shows the UV–vis spectra of the different samples. The presence of iron is associated with an absorption band in the visible region (above 400 nm). Such absorption band increases with the iron content and the annealing temperature. This observation is consistent with the color change of the samples. Apparently, two components contribute to this absorption enhancement in the visible region. The two contributions originate on the presence of Fe^{3+}. The excitation of Fe^{3+} 3d electrons into the TiO_2 conduction band (charge transfer transition) takes place at 415 nm, according to the energy levels proposed [22]. In addition, a broad band centered at 500 nm has been ascribed to the d–d transition of Fe^{3+} or to the charge transfer transition between iron ions ($Fe^{3+} + Fe^{3+} \rightarrow Fe^{4+} + Fe^{2+}$) [4,9,22].

3.3. EPR

The EPR spectra from the iron-loaded catalysts annealed at different temperatures are shown in Fig. 4. Two main resonance bands, corresponding to iron cations, are clearly discerned in all

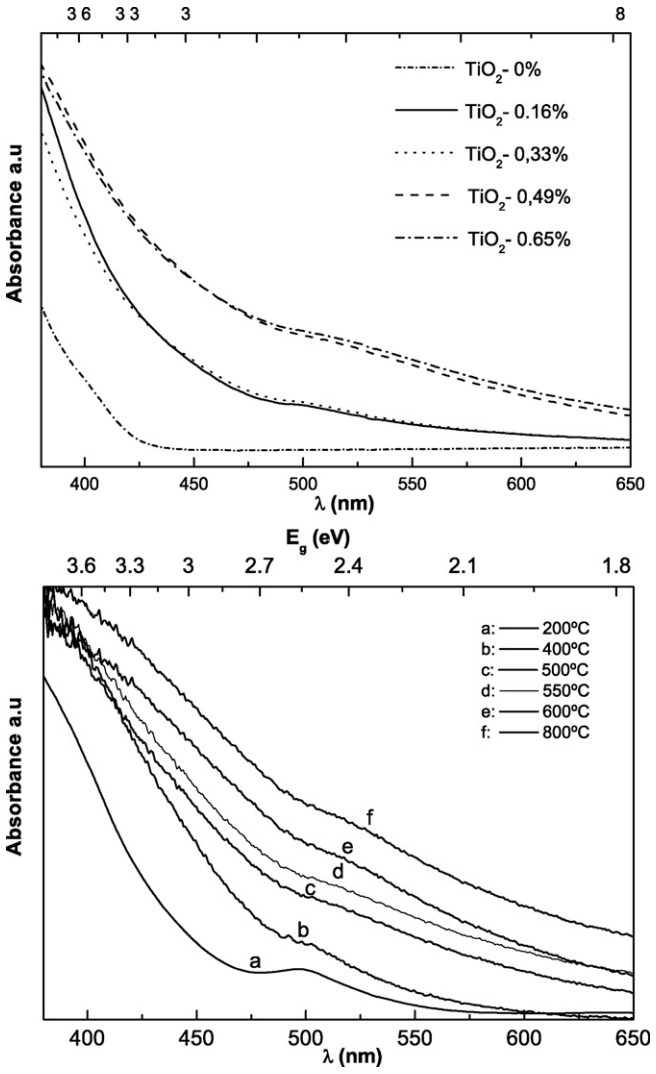

Fig. 3. (Top) UV–vis DRS of samples with different Fe contents (0%$_{at}$, 0.16%$_{at}$, 0.33%$_{at}$, 0.49%$_{at}$, 0.65%$_{at}$). (Bottom) UV–vis DRS spectra of TiO_2-Fe (0.49) sample at different heating temperatures (200, 400, 500, 550, 600, 800 °C).

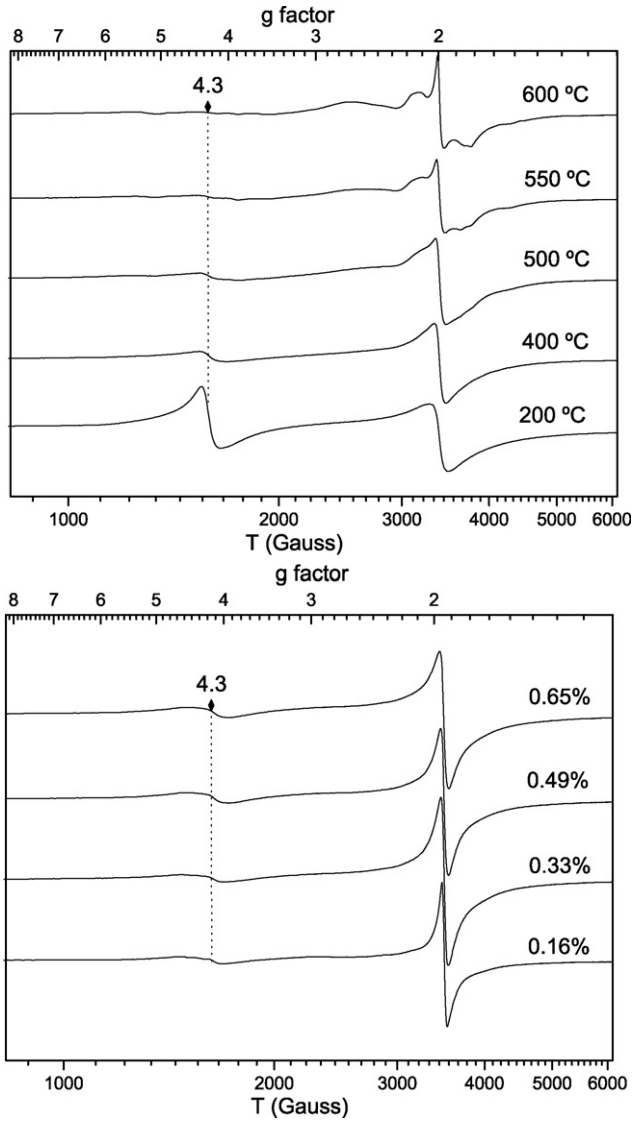

Fig. 4. (Top) EPR spectra recorded at 77 K for TiO_2-Fe (0.49) at different heating temperatures (200, 400, 500, 550, 600, 800 °C). (Bottom) Spectra of the iron-loaded samples calcined at 550 °C (0%$_{at}$, 0.16%$_{at}$, 0.33%$_{at}$, 0.49%$_{at}$, 0.65%$_{at}$).

the spectra. These bands appear at gyromagnetic factors $g = 4.3$ and 2.00 [23–25]. The former is usually assigned to a high spin configuration with a strongly distorted rhombic environment located in the anatase phase. Some authors have argued that this signal is related to oxygen vacancies and/or due to the presence of iron cations into an orthorhombic structure such as brookite [26,27]. Note that the $g = 4.3$ resonance band increases with the iron content. This trend is in good agreement with the idea that substitutional incorporation of iron cations introduces oxygen vacancies in the titania lattice. This resonance peak markedly diminishes as the annealing temperature is increased. Previous EPR studies on Fe-impregnated rutile samples observed the $g = 4.3$ resonance to develop when applying a thermal treatment. The authors associated such a trend to the diffusion of iron ions from their initial location at the titania surface towards the oxide lattice [21]. We associate the opposite trend observed in the present work to a partial surface segregation of the iron ions with the annealing process. Note that in the present case, the dopant is intimately mixed from the very beginning with the amorphous gel. The annealing process crystallizes the titanium oxide and promotes the diffusion and segregation of the iron species. This assumption is

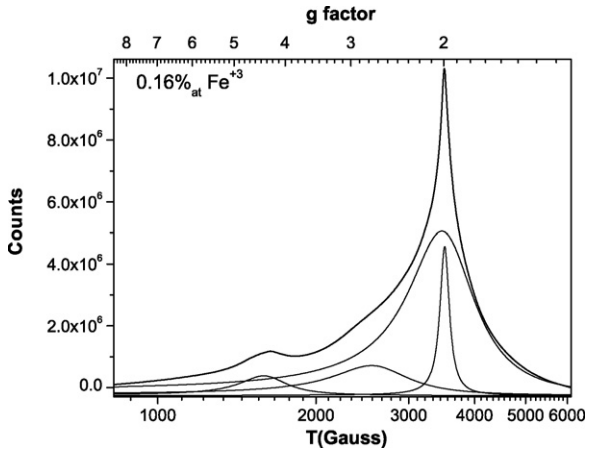

Fig. 5. Integrate form of TiO_2-Fe (0.16) EPR spectrum and the corresponding deconvolution with Lorentzian functions.

also based on the UV–vis results obtained for samples annealed at different temperatures. As mentioned above, the UV–vis spectrum evolved with temperature increasing absorption in the range of 500 nm. We associated this absorption band to the charge transfer transition between iron cations. Indeed, as we increase the calcinations temperature, iron cations tend to segregate to the surface, thus increasing the probability of occurrence of the transition.

The evolution with the heating temperature of the $g = 4.3$ resonance peak can be correlated with that of the $g = 2.00$ band. This band originates from two overlapped resonance peaks [25]: (i) a broad resonance peak corresponding to non-isolated Fe cations, which is usually assigned to the presence of iron oxide or pseudobrookite phases [22,25] and (ii) A narrow resonance peak corresponding to isolated Fe^{3+} cations coordinated with octahedral symmetry in substitutional sites of the anatase lattice.

As the annealing temperature increases, both contributions to the $g = 2.00$ band become more differentiated. At the same time, a slight broadening of the $g = 2$ signal is clearly appreciated when increasing the iron content (Fig. 4, bottom).

In order to deconvolute the different contributions to the $g = 2$ resonance band, the integration forms of the EPR spectra were fitted with Lorentzian functions. As an example, in Fig. 5, the integration form of the EPR spectrum of the 0.16%$_{at}$. Fe^{3+} sample and its corresponding simulation are shown. These fittings reveal the presence of a broad band at around g = 2.9. This rarely reported resonance band originates from ferromagnetic couplings of nearby iron cations. EPR analysis at different temperature was made in order to corroborate that the evolution of the resonance corresponding to these centers does not follow a Curie law [24,28].

Fig. 6 (top) shows the deconvoluted areas of the two resonance peaks having a contribution on the $g = 2$ band. While the area of the narrow peak remains practically constant with the iron content, the area of the broad peak, corresponding to non-isolated Fe^{3+} centers, increases with the addition of iron. This trend suggests that an increase on the iron concentration, far from augmenting the density of isolated cations, promotes the segregation of iron-based compounds.

Another important aspect to put under study is the evolution of the peak width. In an EPR spectrum, the peak width is related to the relaxation time of the spin transition, which is inversely proportional to the width of the resonance (ΔH). Two separated mechanism are involved in this phenomenon: the spin–lattice and the spin–spin relaxation. The former one describes the temperature-dependent interaction of an electron in an excited energy level with the lattice phonons. The latter mechanism consists in an energy transfer from an electron in an upper spin level

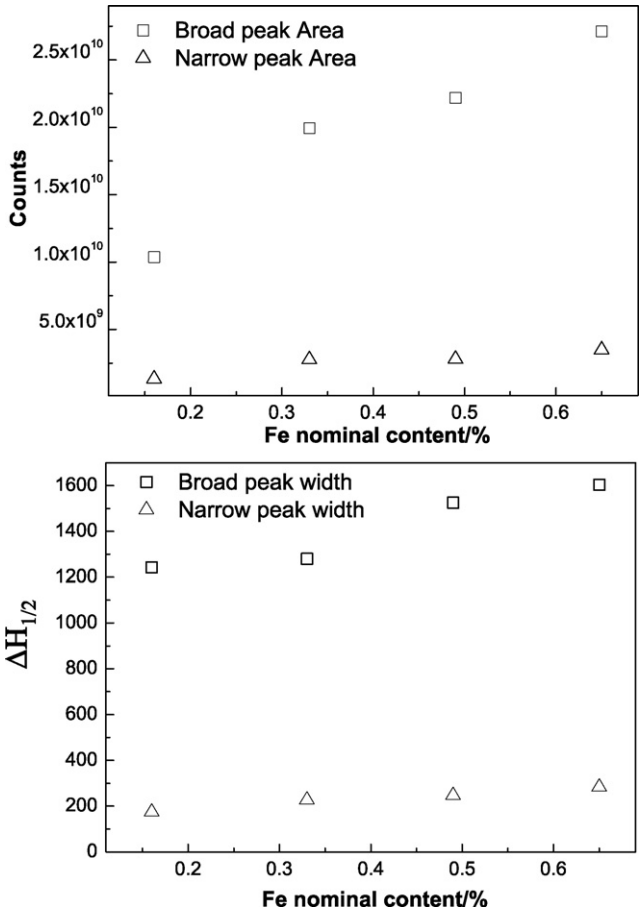

Fig. 6. (Top) Evolution of the area of the two Lorentzian functions at $g = 2.00$ with iron content. (Bottom) Half-width evolution with iron content (0%$_{at}$, 0.16%$_{at}$, 0.33%$_{at}$, 0.49%$_{at}$, 0.65%$_{at}$).

to an electron in a lower spin level. For this last mechanism to take place, the paramagnetic centers must be close to each other. The fitting results (Fig. 6, bottom) suggest that the iron loading only affects the width of the broad peak. This experimental result is consistent with the assumption that this peak is directly related to iron centers located in regions with high concentration of iron species, being the spin–spin interactions enhanced by the increase of the iron loading. On the other hand, the fact that the narrow peak width remains practically constant supports our assignation of this resonance to isolated iron cations. That is, the width of this peak is only associated to spin–lattice interactions.

Finally, note that our EPR spectra strongly differ from those previously reported for materials obtained via iron impregnation or solid state methods [29–32]. Discrepancies ultimately arise from the fundamental difference between the two synthesis strategies. When introducing iron after the crystallization of TiO_2, iron cations are mainly located at the oxide surface, and only at high temperatures they are able to diffuse into the lattice. On the other hand, our synthetic route, involving the mixing of the precursors at the molecular level, allows the incorporation of iron cations into the lattice of the different titania phases. During annealing processes at high temperatures, iron cations segregate and a pseudobrookite phase nucleates.

3.4. Photocatalytic activity

The photocatalytic activities towards methylene blue (MB) decomposition of the iron-loaded samples were compared with those obtained for the undoped TiO_2. In Fig. 7, the relative

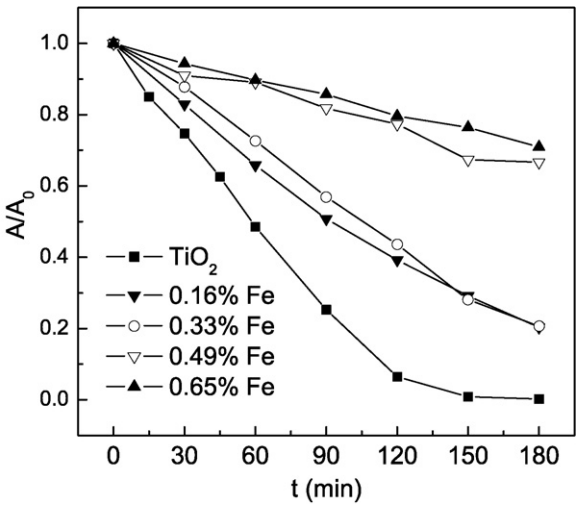

Fig. 7. Kinetics of the photocatalytic decomposition of MB on Fe-doped TiO_2 catalyst (0%$_{at}$, 0.16%$_{at}$, 0.33%$_{at}$, 0.49%$_{at}$, 0.65%$_{at}$).

absorbance decrease with the illumination time of the MB solution containing the Fe-loaded titania is compared with that of the MB solution containing pure titania. Note that the highest rate of MB decomposition was obtained from the solution containing pure titania. Furthermore, the photocatalytic activity towards MB decomposition decreased with the amount of Fe added. These results contrast with those reported by other authors who stated that the addition of Fe remarkably improved the titania photocatalytic activity [33,34]. Such an activity enhancement was explained by the extended lifetimes of electrons and holes due to the double Fe^{3+} role, as a hole and electron trap [3]:

$$Fe^{3+} + e_{cd}^{-} \rightarrow Fe^{2+} \quad \text{electrontrap} \tag{1}$$

$$Fe^{2+} + Ti^{4+} \rightarrow Fe^{3+} + Ti^{3+} \quad \text{migration} \tag{2}$$

$$Fe^{3+} + h_{vb}^{+} \rightarrow Fe^{4+} \quad \text{holetrap} \tag{3}$$

$$Fe^{4+} + OH^{-} \rightarrow Fe^{3+} + OH^{\bullet} \quad \text{migration} \tag{4}$$

For these reactions to proceed, they must take place at or near the particle surface. Thus, the localization of the Fe^{3+} cations inside the oxide lattice inhibits its role on the photocatalytic process by blocking the transfer of trapped charge to the reaction sites. Lattice Fe^{3+} cations are more likely to act as electron–hole pair recombination centers:

$$Fe^{2+} + h_{vb}^{+} \rightarrow Fe^{3+} \quad \text{recombination} \tag{5}$$

$$Fe^{4+} + e_{cd}^{-} \rightarrow Fe^{3+} \quad \text{recombination} \tag{6}$$

$$Fe^{4+} + Fe^{2+} \rightarrow 2Fe^{3+} \quad \text{recombination} \tag{7}$$

$$Fe^{4+} + Ti^{3+} \rightarrow Fe^{3+} + Ti^{4+} \quad \text{recombination} \tag{8}$$

Fig. 8 shows the photocatalytic activity of a TiO_2 sample doped with 0.49% Fe^{3+} and annealed at different temperatures. Note that the photocatalytic activity decreases with the annealing temperature. The introduction of Fe^{3+} recombination centers does not explain such a photocatalytic decrease with the heating temperature since the amount of iron is the same for all samples. Also, the presence of brookite phase, which is not active for photo degradation, cannot explain these results because the brookite-anatase ratios decrease with temperature. One first explanation to such an activity decrease is the reduction of the titania surface area with the annealing process due to the crystallographic domains growth, confirmed by the specific surface area measurements collected in Table 1. A second factor which we believe behind the photocatalytic activity decrease with the annealing temperature is the

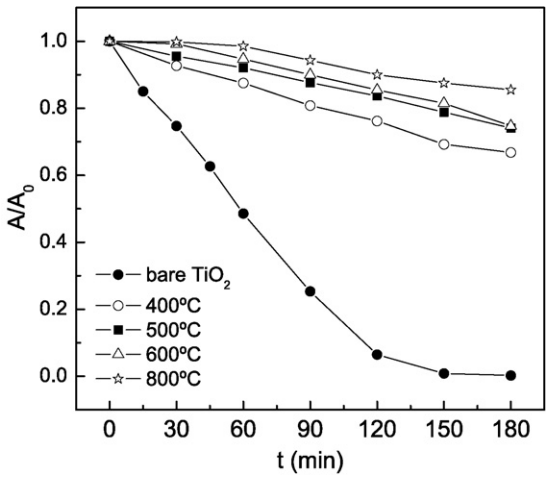

Fig. 8. Kinetics of the photocatalytic decomposition of MB on Fe-doped TiO_2 ($0.49\%_{at.}$) catalyst heated at different temperatures (400, 500, 600, 800 °C).

surface segregation of iron and the formation of iron-based structures, such as iron titanate or pseudobrookite. These composites are highly inactive as a photocatalyst [7,35] and occupy surface sites at the titania surface, thus reducing the concentration of catalytic active sites.

4. Conclusions

In this work, iron-doped titania has been prepared by a sol–gel process from the hydrolysis of alkoxides. XRD characterization indicated that the presence of dopant ions controls the crystallographic domain size, introduces a brookite phase and influences the phase evolution during the annealing process. Segregation of iron in pseudobrookite form was inferred in samples annealed at 800 °C. EPR spectroscopy corroborated the presence of iron-rich secondary phases after temperature annealing processes and provided information regarding the nature and the extent of dopant incorporation. Finally, photocatalytic measurements showed that the introduction of iron as a dopant by co-precipitation of the titanium and iron precursors, far from improving the TiO_2 performance, decreased the activity towards methylene blue degradation. We associated such a decrease with the formation of inactive iron centers in the oxide lattice and the segregation at high temperature of inactive iron-based phases at the titania surface. Our results confirm that the processing of the materials and the dopant incorporation step are extremely important parameters towards improving the photocatalytic activity of wide band gap semiconductors by the introduction of transition metal ions.

Acknowledgements

This work has been partially supported by the Spanish Ministry of Education and Science (MEC) through the projects n-MOSEN (MAT2007-66741-C02-01), CONSOLIDER INGENIO 2009 CDS 00050 MULTICAT and the UE, NanoSciEraConsortium through the project NAWACS (NAN2006-28568-E) and CENIT SOST-CO2 (CEN-2008-1027) of the MCINN. The authors appreciate the access to the Scientific and Technical Services (SCT-UB) where most of the characterizations were done. Special thanks to Xavi Illa for his comments and Núria Clós for her implication in EPR measurements. T. Andreu also thanks the DIUE of the Generalitat de Catalunya for the Beatriu de Pinós grant.

References

[1] A. Fujishima, T.N. Rao, D.A. Truk, J. Photochem. Photobiol. C 1 (2000) 1–21.
[2] M.R. Hoffmann, S.T. Martin, W. Choi, D.W. Bahnemann, Chem. Rev. 95 (1995) 69–96.
[3] A.M. Ruiz, G. Sakai, A. Cornet, K. Shimanoe, J.R. Morante, N. Yamazoe, Sens. Actuators B 93 (2003) 509–518.
[4] J.F. Zhu, W. Zheng, H.E. Bin, J.L. Zhang, M. Anpo, J. Mol. Catal. A: Chem. 216 (2004) 35–43.
[5] J.M. Coronado, J. Soria, J.C. Conesa, R. Bellod, C. Adán, H. Yamaoka, V. Loddo, V. Augugliaro, Top. Catal. 35 (2005) 279–286.
[6] X. Li, P.L. Yue, C. Kutal, New J. Chem. 27 (2003) 1264–1269.
[7] K. Ranjit, B. Viswanathan, J. Photochem. Photobiol. A 108 (1997) 73–78.
[8] Z. Zhang, C. Wang, R. Zakaria, J. Ying, J. Phys. Chem. B 102 (1998) 10871–10878.
[9] J.F. Zhu, F. Chen, J.L. Zhang, H.J. Chen, M. Anpo, J. Photochem. Photobiol. A 180 (2006) 196–204.
[10] M. Delarco, C. Martin, V. Rives, V. Sanchezescribano, G. Ramis, G. Busca, V. Lorenzelli, P. Malet, J. Chem. Soc.: Faraday Trans. 89 (1993) 1071–1078.
[11] A. Dieguez, A. Vila, A. Cabot, A. Romano-Rodriguez, J.R. Morante, J. Kappler, N. Barsan, U. Weimar, W. Gopel, Sens. Actuators B 68 (2000) 94–99.
[12] S.N. Towle, J.R. Bargar, G.E. Brown, G.A. Parks, J. Colloid Interface Sci. 187 (1997) 62–82.
[13] U. Diebold, Surf. Sci. Rep. 48 (2003) 53–229.
[14] L. Kundakovic, M. Flytzani-Stephanopoulos, J. Catal. 179 (1998) 203–221.
[15] J.A. Navío, G. Colón, M. Macías, C. Real, M.I. Litter, Appl. Catal. A 177 (1999) 111–120.
[16] J.A. Wang, R. Limas-Ballesteros, T. López, A. Moreno, R. Gómez, O. Novaro, X. Bokhimi, J. Phys. Chem. B 105 (2001) 9392–9698.
[17] J.A. Navío, G. Colón, M. Trillas, J. Peral, X. Domènech, J.J. Testa, J. Padrón, D. Rodríguez, M.I. Litter, Appl. Catal. B 16 (1998) 187–196.
[18] A. Cabot, A. Dieguez, A. Romano-Rodriguez, J.R. Morante, N. Barsan, Sens. Actuators B 79 (2001) 98–106.
[19] M.I. Litter, J.A. Navío, J. Photochem. Photobiol. A 98 (1996) 171–181.
[20] A. Houas, H. Lachheb, M. Ksibi, E. Elaloui, C. Guillard, J.-M. Herrmann, Appl. Catal. B 31 (2001) 145–157.
[21] A.M. Ruiz, A. Cornet, J.R. Morante, Sens. Actuators B 100 (2004) 256–260.
[22] T. Umebayashi, T. Yamaki, H. Itoh, K. Asai, J. Phys. Chem. Solids 63 (2002) 1909–1920.
[23] R. Aasa, J. Chem. Phys. 52 (1970) 3919–3930.
[24] G. Pecchi, P. Reyes, T. López, R. Gómez, A. Moreno, J.L.G. Fierro, A. Martínez-Arias, J. Sol–Gel Sci. Technol. 27 (2003) 205–214.
[25] J. Soria, J.C. Conesa, V. Augugliaro, L. Palmisano, M. Schiavello, A. Sclafani, J. Phys. Chem. A 95 (1991) 274–282.
[26] R. Arroyo, G. Córdoba, J. Padilla, V.H. Lara, Mater. Lett. 54 (2002) 397–402.
[27] R.D. Shannon, J.A. Pask, J. Am. Ceram. Soc. 48 (1965), 391-&.
[28] C. Adan, A. Bahamonde, M. Fernandez-Garcia, A. Martinez-Arias, Appl. Catal. B 72 (2007) 11–17.
[29] A. Amorelli, J.C. Evans, C.C. Rowlands, T.A. Egerton, J. Chem. Soc.: Faraday Trans. 83 (1987) 3541–3548.
[30] R.S. Debiasi, A.A.R. Fernandes, M.L.N. Grillo, J. Am. Ceram. Soc. 76 (1993) 223–225.
[31] T.A. Egerton, E. Harris, E.J. Lawson, B. Mile, C.C. Rowlands, Phys. Chem. Chem. Phys. 3 (2001) 497–504.
[32] J.S. Thorp, H.S. Eggleston, J. Mater. Sci. Lett. 4 (1985) 1140–1142.
[33] M.S. Nahar, K. Hasegawa, S. Kagaya, S. Kuroda, Sci. Technol. Adv. Mater. 8 (2007) 286–291.
[34] M. Zhou, J. Yu, B. Cheng, J. Hazard. Mater. 137 (2006) 1838–1847.
[35] B. Pal, M. Sharon, G. Nogami, Mater. Chem. Phys. 59 (1999) 254–261.